Journal of Luminescence 156 (2014) 192–198

Contents lists available at ScienceDirect

Journal of Luminescence

journal homepage: www.elsevier.com/locate/jlumin

Review

Spectroscopic properties of Sm^{3+}-doped lanthanum borogermanate glass

R. Rajaramakrishna [a], Brian Knorr [b], Volkmar Dierolf [b], R.V. Anavekar [a,*], H. Jain [c]

[a] Department of Physics, Bangalore University, Bangalore 560056, India
[b] Department of Physics, Lehigh University Bethlehem, PA 18015, USA
[c] Department of Materials Science and Engineering, Lehigh University Bethlehem, PA 18015, USA

ARTICLE INFO

Article history:
Received 21 September 2013
Received in revised form
22 July 2014
Accepted 24 July 2014
Available online 14 August 2014

Keywords:
UV-Optical absorption properties
Melt quenching technique
Germanate glass
J–O Analysis
Samarium ions

ABSTRACT

Ultraviolet–visible–near infrared (UV–vis–NIR) absorption and photoluminescence of $(25-x)$ La_2O_3–$25B_2O_3$–$50GeO_2$ glass series have been studied with different concentrations (x=0.1–1.0 wt%) of Sm_2O_3 as an optically active dopant. The values of Judd–Ofelt (JO) parameters (Ω_t) follow the trend $\Omega_2 > \Omega_4 > \Omega_6$. Visible emission and decay times from the $^4G_{5/2}$ level and its relative quantum efficiencies are measured. Intense reddish-orange emission corresponding to $^4G_{5/2} \rightarrow {}^6H_{7/2}$ transition has been observed in these glasses under 488 nm excitation. A decrease in the quantum yield is observed with increasing Sm^{3+} ion concentration beyond 1% doping level.

Contents

1. Introduction

A considerable literature has accumulated regarding the optical and fluorescent properties of rare earth (RE) ions in silicate, borate, phosphate and tellurite glasses [1]. Many fluorescent transitions of rare earth ions of practical importance are initiated from an excited level with a small energy gap; materials with lower phonon energy are often required as a luminescent host to suppress the non-radiative loss and to obtain higher quantum efficiency of the desired fluorescence. Most oxide glasses have large phonon energy (1100 cm^{-1}) due to the stretching vibration of network-forming oxides [2]. It is found that germanate glasses, presumably due to the large mass of Ge, have smaller maximum vibrational frequencies than those shown by silicate, phosphate and borate glasses. The reduced phonon energy increases the quantum efficiency of luminescence from excited states of RE ions in these matrices and provides incentive for developing a more efficient medium for optical lasers and fiber optical amplifiers [3,4]. The phonon energy of germanate glasses is intermediate between that of silicate and fluoride glasses. In lanthanide doped glasses and crystals the highest energy phonons exercise the most influence on non-radiative relaxations because multiphonon decay occurs with the fewest number of phonons to bridge the energy

* Corresponding author. Tel.: +91 8022961473.
E-mail address: anavekar_271@yahoo.co.in (R.V. Anavekar).

http://dx.doi.org/10.1016/j.jlumin.2014.07.021
0022-2313/

gap. Further lanthanum boro-germanate (LBG) glasses also known for good optical quality with high concentration of rare-earth oxides for laser and related applications [5].

Among active rare-earth ions Sm^{3+} exhibits high solubility in germanate glasses, which also possess excellent physiochemical properties. $LaBGeO_5$ is a model material that is being developed for several photonic applications. It is one of the few oxides that forms glass easily, devitrifies congruently, and then becomes ferroelectric upon crystallization [6]. It is being considered as a potential laser host matrix, and for use in nonlinear optical devices, optical fiber cores and as a recording medium for random-access memory in optoelectronics [7–9]. Accordingly, in this work we have investigated the optical properties of lanthanum borogermanate as a model germanate glass system. In order to determine its potential as a laser host material, we have measured its absorption spectra, radiative transition probabilities, and branching ratios with varying Sm^{3+} concentration.

2. Experimental

$x Sm_2O_3$–$(25-x)La_2O_3$–$25B_2O_3$–$50GeO_2$ (LBG) glasses were prepared with $x=0.1$(S0), 0.5(S1), 1.0(S2), and 2.0(S3) wt%, by a melt-quenching method. The starting batch was prepared by mixing appropriate ratio of high purity H_3BO_3 (Alfa Aesar 99.99%), GeO_2 (Alfa Aesar 99.99%), La_2O_3 (Alfa Aesar 99.99%) and Sm_2O_3 (Stanford Research Laboratory 99.999%) as powders. It was melted in a high purity alumina crucible at 1300 °C in air. This base glass was doped with different concentrations of Sm_2O_3 (ranging from 0.1 to 2 wt%) melted following a similar procedure. The molten glass was cast on preheated brass plate at 200 °C into ~1 mm thick pellets. It was then annealed at 650 °C to relieve stresses, and polished optically flat before spectroscopic characterization.

The Fourier transform infrared spectra (FTIR) of such samples were recorded using a Varian 7000x spectrophotometer. Optical absorption spectra were recorded in the 350–2000 nm wavelength range using a Perkin-Elmer Lambda 7 spectrophotometer. The luminescence spectra were measured over wavelength $\lambda=500$–750 nm under excitation by an argon ion laser operating at 488 nm with a spectral resolution of ± 1.0 nm (Coherent Innova 70). The lifetime measurements were performed using an EKSPLA PL2143B NdYAG pulsed laser as an excitation source and a Lecroy Wave Runner LT584 oscilloscope. All measurements were performed at room temperature. The shape and size of each samples were maintained exactly the same, as well as the excitation beam position and pump carried out to all the samples were kept constant.

The refractive index of the samples was measured at orange wavelength range ($\lambda=635$–590 nm) with a CL-181 jewel refractometer with monobromonaphthalene as the contact layer between the sample and prism. The density of the glass samples was measured following the Archimedes method using toluene as immersion liquid.

3. Results and discussion

3.1. Physical properties

The physical properties of Sm^{3+} doped lanthanum borogermanate (LBG) glasses are presented in Table 1. We note that the molar refractivity (R_M) decreases with increasing samarium content. In general, R_M, which may be considered as a sum of the cationic and oxygen anion refractions, is a measure of bonding among the atoms in glass [10]. The correlation between theoretical optical basicity (Λ_{th}), ($\Lambda_{th}=X_1\Lambda_1+X_2\Lambda_2+X_3\Lambda_3+\ldots+X_n\Lambda_n$) where X_1, X_2, X_3,…X_n are equivalent mole fractions of different oxides, refractive index and electronegativity is important in order to explain the optical behavior of glasses. The polarizability of oxide species depends on the optical basicity of the glass network. Λ represents the ability of oxygen anions to transfer electron density to surrounding cations. It is maximal when these species exist as free O^{2-} ions that have the ability to donate two electrons [11]. However, when oxygen is chemically bonded to surrounding cations in the glass matrix, its charge rendering power to the metal ions decreases. Certain metal ions exhibit changes in color or oxidation state depending on the degree of electronic charge they receive from neighboring oxygen ions. Generally, these ions are p-block metal ions in oxidation states two units less than the number of the group to which they belong [12,13]. Table 1 shows the optical basicity of the present LBG glass series, which increases slightly with Sm^{3+} ion concentration due to increase in polarizability.

3.2. Optical properties

The absorption spectra of the Sm^{3+}-doped lanthanum borogermanate glasses were recorded at room temperature in the wavelength range 350–2000 nm. As an example, the absorption spectrum of the LBGS3 glass is shown in Fig. 1. It exhibits several in-homogeneously broadened bands due to f–f transitions from the ground $^6H_{5/2}$ state to various excited states. The present spectra are similar to those for other reported Sm^{3+}-doped glasses [14–16] and aqua-ions [17]. The absorption bands of the Sm^{3+} ions may be classified into two groups: a lower energy group covering $\lambda=800$–1800 nm, and a higher energy group over $\lambda=320$–650 nm. Fig. 1 shows that the more intense transitions of Sm^{3+} ions are found in the near infrared (NIR) region. The assignment of the bands in the UV–vis region is not easy due to the overlap of different $^{2S+1}L_J$ levels. The transition from the ground $^6H_{5/2}$ state to higher energy ^6H and ^6F terms are spin-allowed ($\Delta S=0$) and hence the transitions lying in the NIR region are intense. The spin-allowed

Table 1
Physical quantities of Sm^{3+} doped LBG glass.

Physical quantities	Data			
	LBGS0	LBGS1	LBGS2	LBGS3
Density, d (g/cm^3)	2.3840	2.5659	2.5853	2.5946
Refractive index (n)	1.776 ± 0.001	1.790 ± 0.001	1.780 ± 0.001	1.770 ± 0.001
Molar refractivity (R_M, cm^3)	8.002 ± 0.001	7.566 ± 0.001	7.477 ± 0.001	7.454 ± 0.001
Polaron radius (r_p, nm)	1.6043	0.9160	0.7254	0.5755
Inter-ionic radius (r_i, nm)	3.9119	2.2324	1.7677	1.4020
Optical basicity (Λ)	0.719	0.723	0.728	0.737
RE ion concentration ($N\times10^{20}$ ions/cm^3)	0.1679	0.9040	1.8210	3.6506
Molar polarizability (α_M, $\times10^{-24}$ cm^3)	12.686	11.994	11.853	11.817
Dielectric constant (ε)	3.154 ± 0.01	3.204 ± 0.01	3.168 ± 0.01	3.133 ± 0.01
Reflection loss (%)	7.81 ± 0.01	8.02 ± 0.01	7.87 ± 0.01	7.73 ± 0.01

$^6H_{5/2} \rightarrow {}^6P_{3/2}$ transition in the UV–vis region is also more intense than the other transitions.

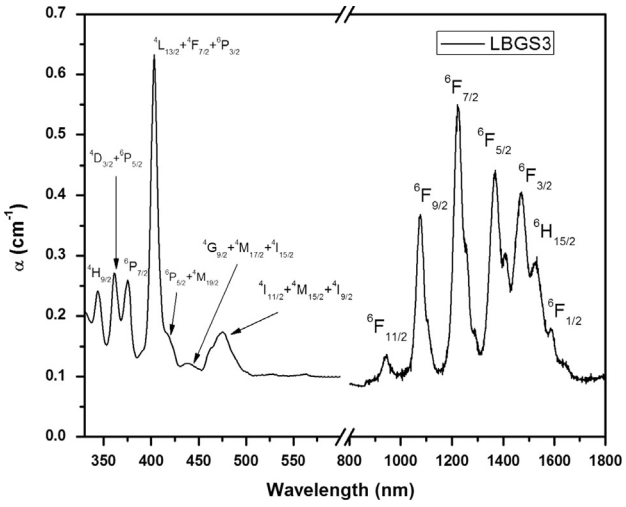

Fig. 1. UV–vis–NIR absorption spectra of Sm^{3+} doped LBG glass.

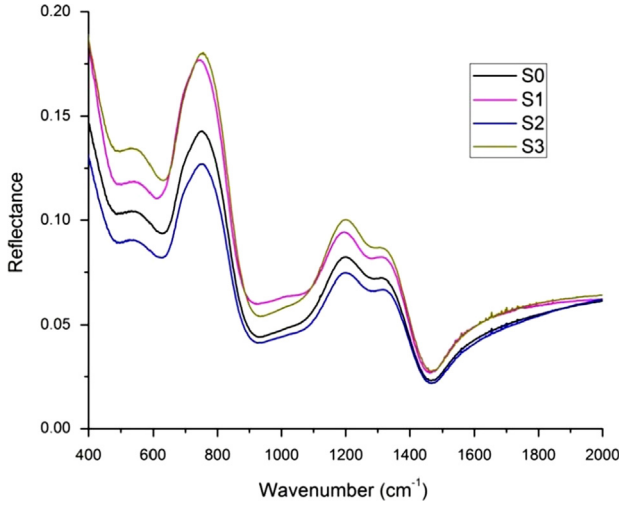

Fig. 2. IR spectra of LBG glass doped with Sm^{3+}.

4. IR spectra

Fig. 2 shows IR spectra of all the glasses of this study. Here the intense bands in the 700–800 cm^{-1} region correspond primarily to stretching vibrations of GeO_4 tetrahedra with a small contribution from vibrations of BO_4 tetrahedra [18]. The latter are completely masked in the spectrum by the broadened and intense peak due to GeO_4. The weak bands in the region 500–700 cm^{-1} characterize bending–stretching vibrations of the chains of BO_4 tetrahedra. According to the spectroscopic description of $LaBGeO_5$ [19,20], the bands in the high-frequency region 1150–1500 cm^{-1} correspond to the vibrations of BO_3 triangles.

5. J–O parameters and radiative properties

The radiative transitions within the $4f^n$ configuration of an Ln^{3+} ion are analyzed by the Judd–Ofelt (JO) theory [21,22]. Accordingly, the calculated oscillator strength, f_{cal}, of an induced electric-dipole absorption transition from an initial state (ΨJ) to final state ($\Psi' J'$) depends on three JO intensity parameters (Ω_t)

$$f_{cal} = \frac{8\pi^2 mc\upsilon}{3h(2j+1)} \frac{(n^2+2)^2}{9n} \sum_{t=2,4,6} \Omega_t (\psi J||U^t||\psi' J')^2 \quad (1)$$

where n is the refractive index of the medium, J is the ground state total angular momentum, υ is the energy of the transition in cm^{-1}, and $||U^t||^2$ are the squared doubly reduced matrix elements of the unit tensor operator [21–23] of the rank $t=2$, 4 and 6. These are calculated from the intermediate coupling approximation for the transition, ΨJ to $\Psi' J'$, at frequency ν (cm^{-1}) and are independent of the host. The experimental oscillator strengths (f_{exp}) of the transitions are obtained by integrating the molar absorptivity $\varepsilon(\nu)$ at wavenumber ν (cm^{-1}) for each band as [24]

$$f_{exp} = 4.32 \times 10^{-9} \int \varepsilon(\upsilon) d\upsilon \quad (2)$$

The Ω_t parameters have been derived from the electric-dipole contribution of the experimental oscillator strengths using least squares fitting. The quality of the fitting is expressed by the least rms deviation Δ_{rms} of the oscillator strength. The experimental and the calculated oscillator strengths of Sm^{3+} and their rms deviations in the precursor LBG glasses with various Sm^{3+} contents are listed in Table 2.

Table 2
Experimental and calculated oscillator strengths ($\times 10^{-6}$) of the Sm^{3+}-doped lanthanum borogermanate glasses.

Transition	Energy	LBGS0		LBGS1		LBGS2		LBGS3	
		f_{exp}	f_{cal}	f_{exp}	f_{cal}	f_{exp}	f_{cal}	f_{exp}	f_{cal}
$^6F_{1/2}$	6297	**3.492**	**3.903**	**3.510**	**3.580**	**4.013**	**3.923**	**3.321**	**3.608**
$^6H_{15/2}$	6531	**0.032**	**0.066**	**0.063**	**0.066**	**0.086**	**0.064**	**0.940**	**0.066**
$^6F_{3/2}$	6811	**4.674**	**4.004**	**5.231**	**5.218**	**5.361**	**5.571**	**6.054**	**5.664**
$^6F_{5/2}$	7326	**2.342**	**2.663**	**6.393**	**5.915**	**6.528**	**6.153**	**7.014**	**6.874**
$^6F_{7/2}$	8196	**9.342**	**9.083**	**10.23**	**10.96**	**10.52**	**10.83**	**11.02**	**11.41**
$^6F_{9/2}$	9306	**6.981**	**7.352**	**8.632**	**7.671**	**7.682**	**7.482**	**8.012**	**7.688**
$^6F_{11/2}$	10,604	**1.398**	**1.249**	**1.942**	**1.262**	**2.435**	**1.227**	**2.578**	**1.252**
$^4I_{11/2} + {}^4M_{15/2} + {}^4I_{9/2}$	21,052	**1.220**	**2.433**	**2.091**	**2.444**	**3.282**	**2.395**	**2.842**	**2.429**
$^4G_{9/2} + {}^4M_{17/2} + {}^4I_{15/2}$	22,831	**0.223**	**0.486**	**0.723**	**0.518**	**0.832**	**0.508**	**1.091**	**0.523**
$^4M_{19/2} + {}^6P_{5/2}$	23,809	**0.2**	**0.502**	**2.201**	**1.386**	**2.678**	**1.431**	**2.870**	**1.640**
$^4L_{13/2} + {}^4F_{7/2} + {}^6P_{3/2}$	24,813	**3.875**	**4.394**	**9.820**	**10.99**	**10.51**	**11.31**	**11.83**	**12.88**
$^6P_{7/2}$	26,666	**4.876**	**3.862**	**4.345**	**3.928**	**4.398**	**3.822**	**4.687**	**3.907**
$^4D_{3/2} + {}^6P_{5/2}$	27,624	**0.91**	**1.38**	**2.974**	**3.660**	**3.107**	**3.780**	**3.675**	**4.328**
$^4H_{9/2}$	29,069	**–**	**–**	**1.521**	**1.058**	**0.984**	**0.074**	**0.941**	**0.776**
N		13	13	14	14	14	14	14	14
Δ_{rms}		**0.559**		**0.610**		**0.681**		**0.715**	
n		1.776		**1.79**		**1.78**		**1.77**	

It has been proposed that in an oxide glass a RE ion is surrounded by eight non-bridging oxygen atoms belonging to the corners of BO_4/PO_4 tetrahedra in borate/phosphate glass, with each tetrahedron donating two oxygens, as shown in Fig. 3 [25].

From the similarity of spectral features in ternary germanate and GeO_2 glasses it appears that the Sm^{3+} ion is situated in a distorted cube formed by four GeO_4 tetrahedra linked at corners. Because of the smaller distance between Sm^{3+} and the surrounding oxygens in GeO_2 glasses, the vibrational coupling between the Sm^{3+} ion and its surrounding medium is stronger, and hence the oscillator strengths are higher in this matrix. In the absorption spectrum of Sm^{3+}:LBG glass, the energy multiplets are very closely spaced and are difficult to resolve with reliable SLJ values. To avoid this difficulty, the matrix elements of all the overlapping transitions in that region are summed and then JO intensity parameters are calculated; the results are presented in Table 3. In general, the Ω_2 parameter is an indicator of the covalency of the metal ligand bond, and Ω_4 and Ω_6 are related to the rigidity of the host matrix [24]. As Ω_2 is sensitive to the covalent bonding, it can be reasonably deduced that the covalent degree of the present LBG glass is higher than any simple glass matrix listed in Table 2. On the other hand, Ω_6 is related to the rigidity, and Ω_4/Ω_6 determines the spectroscopic quality of material [27]. The present glass shows the highest Ω_4/Ω_6 value, indicating the favorable performance as host for luminescence activators.

Ω_2 depends on the asymmetry around the Sm^{3+} ion, which itself is determined by the covalency of the Sm–O bond; a lower symmetry in the vicinity of the rare earth ion results in a higher value of Ω_2 [28,29]. The Ω_4 and Ω_6 Judd–Ofelt parameters determine luminescent properties such as branching ratios and the stimulated emission cross section. They are related to long range parameters that determine the bulk properties of the glass like basicity of the matrix. Ω_6 relates to the density of 6s electrons that shield the 4f electrons responsible for optical transitions of Ln^{3+} ions [24]. Due to the effective shielding of 4f shell by fully filled 5s and 5p orbitals, electronic cloud of trivalent lanthanide ions experiences very weak ligand field influence. Although weak, this perturbation is responsible for the 4f intra-configurational electric dipole transitions, which are otherwise forbidden under Laporte's Rule. Hence intensities of these forced electric dipole 4f transitions reflect the interaction of the rare earth ion with its nearest neighbors. Judd and Ofelt independently proposed a theory for the quantitative estimate of the forced electric dipole transition intensities [21,22]. Among the rare earth ions Sm^{3+} is used as probe and also as an efficient laser active ion with its emission around 600 nm for the lanthanum borogermanate glass.

The radiative properties can be calculated from Ω_t [30], since the spontaneous transition probability is expressed as

$$A(\Psi J, \Psi' J') = A_{ed} + A_{md}, \tag{3}$$

where A_{ed} and A_{md} are the electric and magnetic-dipole contributions, respectively. These are calculated from

$$A_{ed} = \frac{64\pi^4 \upsilon^3}{3h(2J+1)} \frac{n(n^2+2)^2}{9} S_{ed} \text{ and } A_{md} = \frac{64\pi^4 \upsilon^3}{3h(2J+1)} n^3 S_{md} \tag{4}$$

where $n(n^2+2)^2/9$ and n^3 are the local field corrections for the electric dipole and for magnetic dipole transitions, respectively. S_{ed} and S_{md} are the electric and magnetic dipole line strengths, calculated from the following expressions:

$$S_{ed} = e^2 \sum_{t=2,4,6} \Omega_t (\Psi J \| U^t \| \Psi' J')^2 \text{ and } S_{md} = \frac{e^2 h^2}{16\pi^2 m^2 c^2} (\Psi J \| L + 2S \| \Psi' J')^2 \tag{5}$$

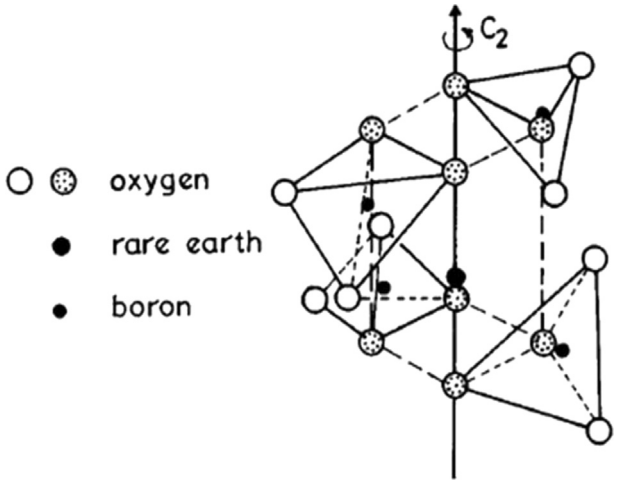

Fig. 3. Nearest oxygen neighbors surrounding the rare earth Ref. [26].

The sum of $A(\Psi J, \Psi' J')$ for the states involved gives the total radiative probability (A_T)

$$A_T(\Psi J) = \sum_{\Psi' J'} A(\Psi J, \Psi' J') \tag{6}$$

where the sum is extended over all states of energy lower than $\Psi' J'$. The radiative lifetime of an emitting state is related to the total spontaneous emission probability for all transitions from this state by

$$\tau_R(\Psi J) = \frac{1}{A_T(\Psi J)} \tag{7}$$

Another important radiative property, the fluorescent branching ratio (β_R) for the different transitions originating from the same excited state, is calculated from the equation

$$\beta_R(\Psi J, \Psi' J) = \frac{A(\Psi J, \Psi' J')}{A_T(\Psi J)} \tag{8}$$

Table 3
Judd–Ofelt ($\times 10^{-20}$cm^2) parameters, trends of Ω_t parameters and spectroscopic quality factor (Ω_4/Ω_6) of the Sm^{3+}-doped lanthanum borogermanate glasses.

Glass composition	JO parameters			Trends of Ω_λ	Ω_4/Ω_6	Ref.
	Ω_2	Ω_4	Ω_6			
LBGS0	**10.69 ± 0.05**	**3.0 ± 0.05**	**7.5 ± 0.05**	$\Omega_2 > \Omega_6 > \Omega_4$	**0.4**	This work
LBGS1	**9.69 ± 0.05**	**8.18 ± 0.05**	**7.46 ± 0.05**	$\Omega_2 > \Omega_4 > \Omega_6$	**1.0**	
LBGS2	**10.71 ± 0.05**	**8.52 ± 0.05**	**7.30 ± 0.05**	$\Omega_2 > \Omega_4 > \Omega_6$	**1.1**	
LBGS3	**9.93 ± 0.05**	**9.84 ± 0.05**	**7.51 ± 0.05**	$\Omega_2 > \Omega_4 > \Omega_6$	**1.3**	
GPBS	8.56	3.02	2.37	$\Omega_2 > \Omega_4 > \Omega_6$		[2]
GeO_2	6.48	4.98	3.18	$\Omega_2 > \Omega_4 > \Omega_6$		[31]
B_2O_3	6.36	6.02	3.51	$\Omega_2 > \Omega_4 > \Omega_6$	–	[31]
P_2O_5	4.31	4.28	5.78	$\Omega_6 > \Omega_2 > \Omega_4$		[31]
TeO_2	3.17	3.65	1.61	$\Omega_4 > \Omega_2 > \Omega_6$		[31]

Table 4
Emission band position (λ_p, nm), effective band width ($\Delta\lambda_{eff}$, nm), radiative transition probability (A, s^{-1}), peak stimulated emission cross-section ($\sigma_P^E \times 10^{-22}$ cm^2), experimental and calculated branching ratios (β_R) for the $^4G_{5/2}$ transition level of Sm^{3+}:LBG glasses.

Transition	Parameters	S0	S1	S2	S3
$^4G_{5/2}\rightarrow{}^6H_{5/2}$	λ_p	563.61	563.61	563.61	563.41
	$\Delta\lambda_{eff}$	9.537	9.48	9.128	7.35
	A	38.09	49.1	49.87	50.94
	σ_P^E	0.441	0.569	0.578	0.59
	β_R(Exp)	0.0439	0.0429	0.0426	0.0425
	β_R(Cal)	0.051	0.065	0.066	0.069
$^4G_{5/2}\rightarrow{}^6H_{7/2}$	λ_p	600.04	600.04	599.78	600.19
	$\Delta\lambda_{eff}$	12.49	12.18	12.88	8.47
	A	290.19	429.82	426.25	455.97
	σ_P^E	1.903	2.821	2.787	2.992
	β_R(Exp)	0.334	0.375	0.364	0.38
	β_R(Cal)	0.44	0.642	0.644	0.697
$^4G_{5/2}\rightarrow{}^6H_{9/2}$	λ_p	647.56	647.29	647.29	645.27
	$\Delta\lambda_{eff}$	17.05	17.1	16.14	7.6
	A	358.85	424.69	447.6	440.25
	σ_P^E	1.815	2.149	2.266	2.232
	β_R(Exp)	0.413	0.371	0.382	0.366
	β_R(Cal)	0.637	0.742	0.791	0.787
$^4G_{5/2}\rightarrow{}^6H_{11/2}$	λ_p	707.22	707.75	706.69	704.31
	$\Delta\lambda_{eff}$	21.64	18.05	18.32	9.99
	A	55.4	105.8	106.32	117.66
	σ_P^E	0.243	0.464	0.467	0.514
	β_R(Exp)	0.0638	0.0925	0.0908	0.0976
	β_R(Cal)	0.118	0.223	0.226	0.252

and is used to predict the relative intensity of the emission lines. Table 4 shows the spontaneous transition probabilities and the branching ratios of the optical transitions for the four Sm^{3+}:LBG glasses from $^4G_{5/2}$ emitting level. The fluorescence branching ratios (β_R) are also presented in Table 4, which shows that the values of A and β_R are much higher for these transitions than for other radiative transitions. The peak-stimulated-emission cross-section, $\sigma(\lambda_p)$ $(\Psi J,\Psi' J')$, between the states ΨJ and $\Psi' J'$ having the probability of $A(\Psi J,\Psi' J')$ can be calculated from

$$\sigma(\lambda_p) = \left(\frac{{\lambda_p}^4}{8\pi c n^2 \Delta\lambda_{eff}}\right) A(\Psi J, \Psi' J') \tag{9}$$

where λ_p is the wavelength of the emission peak and $\Delta\lambda_{eff}$ is the effective line width [24]. The latter is determined by

$$\Delta\lambda_{eff} = \int \frac{I(\lambda)\, d\lambda}{I_{max}} \tag{10}$$

where I is the fluorescence intensity and I_{max} is the intensity at band maximum.

Sm^{3+}-doped LBG glasses emit bright reddish-orange luminescence under 488 nm excitation. The emission spectra of Sm^{3+}:LBG glasses are shown in Fig. 4. They consist of green, yellow and reddish-orange emission bands at 565, 602, 649, and 700 nm, which correspond to the $^4G_{5/2}$–$^6H_{J=5/2,\ 7/2,\ 9/2,\ \text{and}\ 11/2}$ transitions. They have been observed when the glass sample is excited by UV and blue radiation. Broad excitation wavelength range from UV to bluish-green shows that commercial UV and blue laser diodes, blue and bluish-green LEDs and Ar^+ optical laser are powerful pumping sources for Sm^{3+}-doped LBG glass. The 600 nm emission is the most intense band in the present glass. The peak wavelengths (λ_P), bandwidths ($\Delta\lambda_{eff}$), peak emission cross-sections (σ_P) and branching ratios (β_R) of four emission transitions of Sm^{3+} ion are presented in Table 4. Out of the four transitions, the peak emission cross-section is the highest for $^4G_{5/2}$–$^6H_{7/2}$ and $^4G_{5/2}$–$^6H_{9/2}$ transition for all compositions. In general, the luminescence branching ratio is a critical parameter to the laser designer because it characterizes the possibility of attaining stimulated emission from any specific transition. The relative areas under the emission peaks are known as experimental branching ratios (β_R (Exp)) and are compared in Table 4 with those predicted from the JO theory. In the present study, the $^4G_{5/2}$–$^6H_{7/2}$ transition shows higher β_R values, and the same trend has been noticed in lead germanate glasses [32]. Moreover, the measured branching ratios are found to be nearly 7%, 50%, and 35% for the transitions $^4G_{5/2}$–$^6H_{5/2}$, $^4G_{5/2}$–$^6H_{7/2}$ and $^4G_{5/2}$–$^6H_{9/2}$ respectively. Since the total branching ratio contributed from these transitions is more than 92% one can expect intense visible emissions for Sm^{3+} ions in lanthanum borogermanate glasses. As a result these glasses are expected to be promising material for visible lasers.

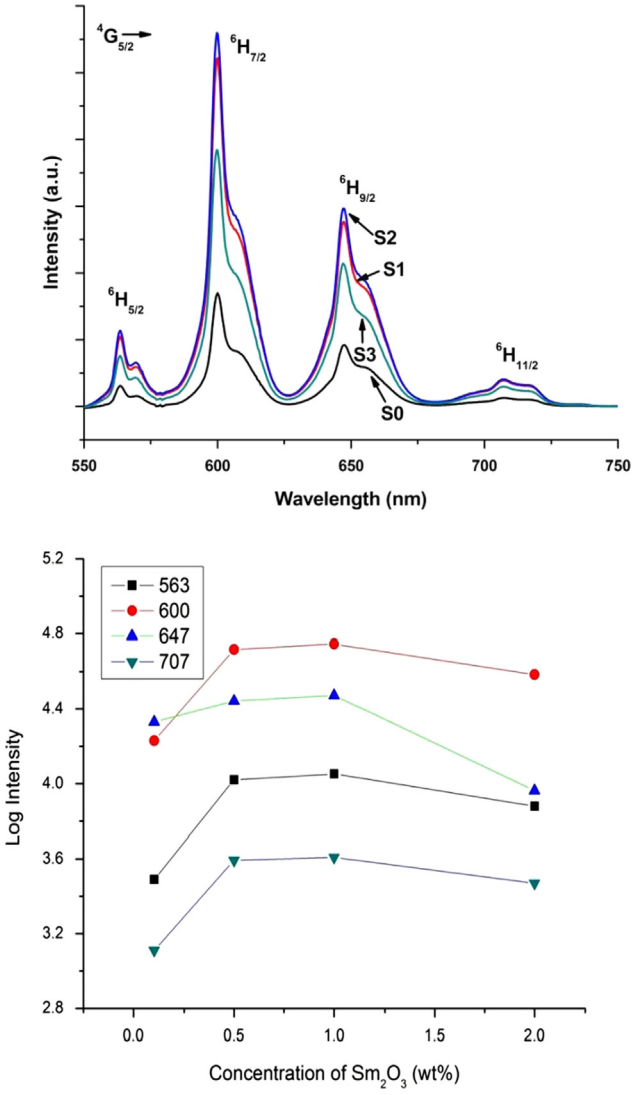

Fig. 4. Emission spectra of Sm_2O_3 doped LBG glasses and Sm_2O_3 concentration dependence of intensity.

The intensity of all fluorescence bands decreases as the concentration of Sm_2O_3 increases beyond 1.0 wt%. It indicates concentration quenching by cross relaxation (CR) processes. Comparing the ionic radius (r) of the Sm^{3+} ion (r=1.09 Å in CN=8 with mean inter-ionic distance, r_i=1.40 nm) and polaron radius, r_p=0.57 nm, for the 2.0 wt% Sm_2O_3 sample (Table 1), the CR processes appear to be responsible for the decrease in intensity of the bands due to close proximity of the Sm^{3+}–Sm^{3+} ion pair (CR starts when the mean distance between ions approaches ~15 Å and the concentration is greater than 12×10^{19} ions/cm^3) [34]. It reveals that the highest intensity of the $^4G_{5/2}$–$^6H_{7/2}$ transition is for 1.0 wt% Sm_2O_3. This fact is depicted in

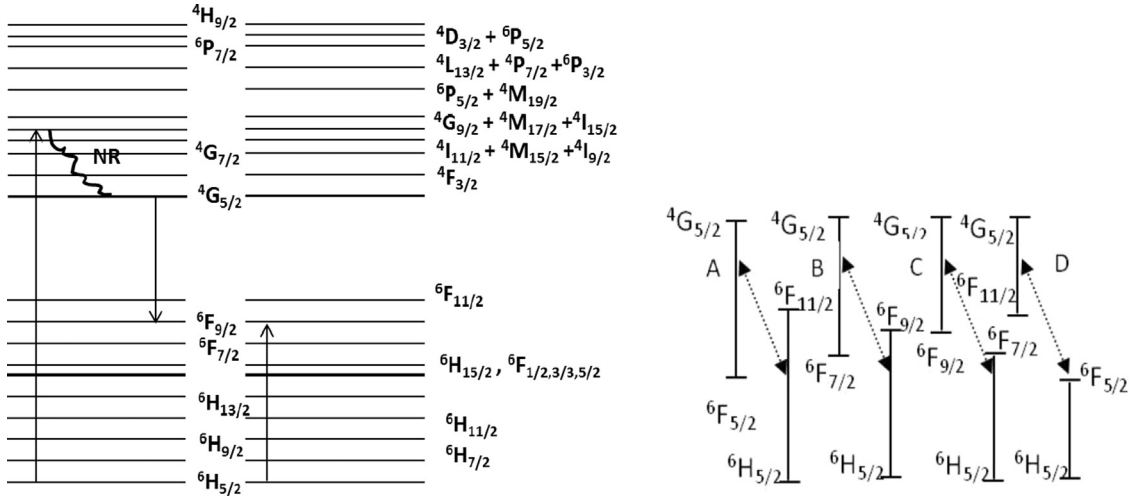

Fig. 5. Partial energy level diagram of Sm^{3+}; the main CR channels between the $^4G_{5/2}$ and $^6H_{5/2}$ levels are also shown separately.

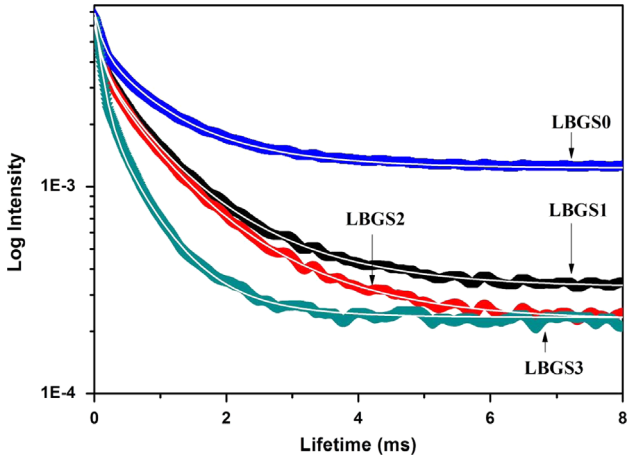

Fig. 6. Decay curves for the $^4G_{5/2}$ level of Sm^{3+}:LBG glasses.

Fig. 5. It also suggests the involvement of an energy transfer (ET) process at relatively higher concentrations of active ions.

The lifetime, τ, of Sm^{3+}:LBG glasses was measured and compared with other phosphate and germinate glasses. The quenching of lifetime and non-exponential behavior of the decay profile shown in Fig. 6 are due to the non-radiative electronic transition (ET) between Sm^{3+} ions. The measured lifetimes of the $^4G_{5/2}$ level for different concentrations are shown in Table 5, from which it is clear that the Sm^{3+}:LBG glasses show almost similar efficiencies when compared with other samarium-doped glasses. The relative quantum yield of the luminescence has been obtained at different concentrations and shown in Fig. 7. The error in the calculation of the quantum yield is shown by error bars. The value of quantum efficiency (η) is more than 1 for lower concentration which is attributed due to the error based on the Δ_{rms} value (see Table 2). The efficiency in these glasses can be explained by stronger cross-relaxation (see Fig. 5) (resulting in non-radiative losses) between neighboring Sm^{3+} ions in the matrix. The mechanism of such a cross-relaxation process is as follows [35]:

$$(^4G_{5/2} \rightarrow {}^6F_{9/2}) \rightarrow (^6H_{5/2} \rightarrow {}^6F_{9/2})$$

Or

$$(Sm^{3+}{}^4G_{5/2})* + (Sm^{3+}{}^6H_{5/2}) \rightarrow 2(Sm^{3+}{}^6F_{9/2})*$$

Table 5
Experimental (τ_{exp}) and radiative (τ_{rad}) lifetimes (ms), and quantum efficiency (η) of the Sm^{3+}:LBG glasses.

Glasses	τ_{exp} (ms)	τ_{rad} (ms)	η	Ref.
LBGS0	1.027	**1.152**	**0.89**	Present work
LBGS1	0.782	**0.874**	**0.89**	
LBGS2	0.736	**0.854**	**0.86**	
LBGS3	0.428	**0.833**	**0.51**	
$55P_2O_5$–39.9PbO–$5Nb_2O_5$–0.1Sm	2.554	–	1.02	
$55P_2O_5$–39.5PbO–$5Nb_2O_5$–0.5Sm	2.277	–	0.85	
$55P_2O_5$–39PbO–$5Nb_2O_5$–1.0Sm	1.896	2.820	0.69	[24]
$55P_2O_5$–38PbO–$5Nb_2O_5$–2.0Sm	1.386	–	0.45	
$55P_2O_5$–36PbO–$5Nb_2O_5$–4.0Sm	0.829	–	0.26	
50 GeO_2–43PbO–$5PbF_2$–$2SmF_3$	1.084	2.177	0.49	[2]
49PbO–50GeO_2–1.0Sm	1.130	1.653	0.68	[32]
49PbO–30GeO_2–20Ga–1.0Sm	1.060	1.740	0.60	[32]
49PbO–30GeO_2–20B_2O_3–1.0Sm	1.340	2.117	0.63	[32]
49PbO–30GeO_2–20TeO_2–1.0Sm	0.794	1.550	0.51	[33]

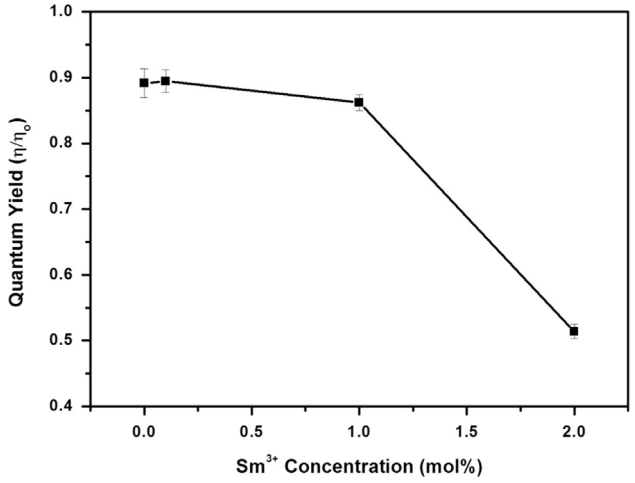

Fig. 7. Variation of quantum efficiency with concentration of Sm^{3+} ions in LBG glasses.

(A): [$^4G_{5/2}$, $^6H_{5/2}$]→[$^6F_{5/2}$, $^6F_{11/2}$] (~10,400 cm^{-1}). This cross-relaxation is due to energy transfer from the excited $^4G_{5/2}$ emission level to the nearby Sm^{3+} ions in the ground level $^6H_{5/2}$. It occurs through $^4G_{5/2} \rightarrow {}^6F_{5/2}$ transition on one ion and $^6H_{5/2} \rightarrow {}^6F_{11/2}$ transition on the other. After that, both ions quickly decay nonradiatively

Table 6
Radiative properties of $^4G_{5/2} \rightarrow {}^6H_J$ transitions in LBGSm1 and LBGSm2 glasses.

Radiative properties	LBGSm1 $^4G_{5/2}\rightarrow$				LBGSm2 $^4G_{5/2}\rightarrow$			
	$^6H_{5/2}$	$^6H_{5/2}$	$^6H_{9/2}$	$^6H_{11/2}$	$^6H_{5/2}$	$^6H_{5/2}$	$^6H_{9/2}$	$^6H_{11/2}$
Peak wavelength (nm)	563	599	647	706	563	599	647	706
Effective band width ($\Delta\lambda_{eff}$) (nm)	**9.48**	**12.18**	**17.10**	**18.05**	**9.128**	**12.88**	**16.14**	**18.32**
Stimulated emission cross-section ($\sigma_P^E \times 10^{-22}$ cm^2)	**0.569**	**2.821**	**2.149**	**0.464**	**0.578**	**2.787**	**2.266**	**0.467**
Gain band width ($(\sigma_e \times \Delta\lambda_{eff}) \times 10^{-28}$ cm^3)	**0.539**	**3.435**	**3.674**	**0.837**	**0.527**	**3.589**	**3.657**	**0.855**
Optical gain ($(\sigma_e \times \tau_R) \times 10^{-25}$ cm^2 s)	**0.471**	**2.465**	**1.878**	**0.405**	**0.493**	**2.380**	**1.935**	**0.398**

to the ground state. The energy resonance of these transitions and other possible transitions: (B): [$^4G_{5/2}$, $^6H_{5/2}$]→[$^6F_{7/2}$, $^6F_{9/2}$] (~9500 cm^{-1}); (C): [$^4G_{5/2}$, $^6H_{5/2}$]→[$^6F_{9/2}$, $^6F_{7/2}$] (~8400 cm^{-1}) and (D): [$^4G_{5/2}$, $^6H_{5/2}$]→[$^6F_{11/2}$, $^6F_{5/2}$] (~7100 cm^{-1}) is illustrated in Fig. 4. These processes are responsible for a nonradiative depopulation of the $^4G_{5/2}$ level from which florescence occurs. Since germanate glasses have lower phonon energies than the conventional phosphate, silicate and borate glasses, and since the nonradiative losses are proportional to the phonon energies, we can expect that these glasses would be suitable as laser host material for various RE ions which have small energy gaps between the lasing and the next lower level. Due to high concentration of GeO_2 in the present matrix, enhanced probability of cross-relaxation causing nonradiative losses, stability, and transparency of lanthanum borogermanate glasses gives distinct advantages over other glasses.

The stimulated emission cross-section (σ_e) has been used to identify the potential laser transitions of rare earth ions in any host matrix—a good laser transition should have large stimulated emission cross-section. The large stimulated-emission cross sections are the attractive feature for low-threshold, high-gain, laser applications, which are utilized to obtain CW laser action [33]. LBGSm2 glass shows large emission cross-sections (σ_P) values compared with remaining LBG glasses doped with different concentrations.

The gain bandwidth ($\sigma_e \times \Delta\lambda_p$) and optical gain ($\sigma_e \times \tau_R$) parameters are critical to predict the amplification of the medium in which the rare earth ions are situated. A good optical amplifier should have large σ_e, ($\sigma_e \times \Delta\lambda_p$) and ($\sigma_e \times \tau_R$) values. The values are presented in Table 6. Reasonably present glasses showing higher values of these parameters for $^4G_{5/2}\rightarrow{}^6H_{7/2}$ and $^6H_{9/2}$ transition suggest that the LBGSm2 glass is a suitable candidate for reddish-orange laser applications. The transition $^6H_{9/2}$ shows higher value due to its gain bandwidth, which is high compared to that for $^6H_{7/2}$.

6. Conclusions

Judd–Ofelt parameters are calculated from the absorption spectrum of LBG:Sm glasses. These parameters are used to determine the radiative properties for the $^4G_{5/2}$ fluorescent level. The Ω_t values follow the same trend $\Omega_2 > \Omega_4 > \Omega_6$ as for other Sm^{3+} doped germanate or other oxide glasses. Intense reddish-orange emission corresponding to $^4G_{5/2}\rightarrow{}^6H_{7/2}$ transition has been observed in these glasses under 488 nm excitation, and has been observed when the glass sample was excited by UV radiation. Reasonably high radiative properties of $^4G_{5/2}\rightarrow{}^6H_{7/2}$ transition suggest that the LBGSm2 glass is also a suitable candidate for reddish-orange laser applications. The decrease in the quantum yield with increasing Sm doping supports the increase in ET between Sm^{3+} ions with increasing dopant concentration. Therefore, these glasses are suitable as laser host materials. The intensity of all fluorescence bands decreases as the concentration of Sm_2O_3 increases beyond 1.0 wt%. The predicted radiative properties for the levels are highly useful to establish new laser channels experimentally for Sm^{3+} ions.

Acknowledgment

The authors thank IMI-NFG for initiating our international collaboration via research exchange visits (NSF, USA Grant DMR-0844014). The work at Bangalore University is supported by DAE-BRNS (No. 2010/34/25/BRNS/1161). We also thank Prof C.K. Jayashankar for his valuable discussion on JO Analysis.

References

[1] D.D. Martino, L.F. Santos, A.C. Marques, R.M. Almeida, J. Non-Cryst. Solids 394 (2001) 293.
[2] B. Klimez, G. Dominiak-Dzik, P. Solarz, M. Zelechower, W.R. Romanowski, J. Alloys Compd. 403 (2005) 76.
[3] Y. Wang, J. Ohwaki, Appl. Phys. Lett. 63 (1993) 3268.
[4] G. Lakshminarayana, J. Qiu, M.G. Brik, G.A. Kumar, I.V. Kityk, J. Phys. Condens. Matter 20 (2008) 375104.
[5] V.N. Sigaev, S.V. Lotarev, E.V. Orlova, S.Yu. Stefanovich, P. Pernice, A. Aronne, E. Fanelli, I. Gregora, J. Non-Cryst. Solids 353 (2007) 1956.
[6] P. Gupta, H. Jain, D.B. Williams, R. Kuechler, O. Kanert, J. Non-Cryst. Solids 349 (2004) 291.
[7] I. Chakraborty, J. Shelby, R. Condrate, J. Am. Ceram. Soc. 67 (1984) 782.
[8] T. Kikacheishvili, N. Papunashvili, N. Sikharulidze, I. Tsagareishvili, Glass Phys. Chem. 28 (2002) 229.
[9] I. Chakraborty, D. Day, J. Am. Ceram. Soc. 68 (1985) 641.
[10] J. Kreidl, Glastech. Ber. 62 (1989) 213.
[11] V. Dimitrov, T. Komatsu, J. Non-Cryst. Solids 249 (2–3) (1999) 160.
[12] A. Lebouteiller, P. Courtine, J. Solid State Chem. 137 (1) (1998) 94.
[13] J.A. Duffy, J. Non-Cryst. Solids 297 (2–3) (2002) 275.
[14] S. ShanmugaSundari, K. Marimuthu, M. Sivaraman, S. SurendraBabu, J. Lumin. 130 (2010) 1313.
[15] Tirtha Som, Basudeb Karmakar, J. Lumin. 128 (2008) 1989.
[16] A.A. Ali, J. Lumin. 129 (2009) 1314.
[17] W.T. Carnall, P.R. Fields, K. Rajnak, J. Chem. Phys. 49 (1968) 4424.
[18] V.N. Sigaev, S.V. Lotarev, E.V. Orlova, N.V. Golubev, V.V. Koltashev, V.G. Plotnichenko, G.A. Komandin, Glass Ceram. 67 (2010) 3.
[19] A. Rulmont, P. Tarte, J. Solid State Chem. 75 (1988) 244.
[20] A.M. Efimov, J. Non-Cryst Solids 253 (1999) 95.
[21] B.R. Judd, Phys. Rev. 127 (1962) 750.
[22] G.S. Ofelt, J. Chem. Phys. 37 (1962) 511.
[23] C.K. Jayasankar, E. Rukmini, Opt. Mater. 8 (1997) 193.
[24] R. Praveena, V. Venkatramu, P. Babu, C.K. Jayashankar, Physica B 403 (2008) 3527.
[25] M. Das, K. Annapurna, P. Kundu, R.N. Dwivedi, S. Buddhudu, Mater. Lett. 60 (2006) 222.
[26] R. Reisfeld, Y. Eckstein, J. Solid State Chem. 5 (1972) 174.
[27] P.R. Watekar, S. Ju, W.T. Han, J. Non-Cryst. Solids 354 (2008) 1453.
[28] M.B. Saisudha, J. Ramakrishna, Phys. Rev. B. 53 (1996) 6186.
[29] N.B. Shigihalli, R. Rajaramakrishna, R.V. Anavekar, Can. J. Phys. 91 (2013) 322.
[30] W.T. Carnall, P.R. Field, K. Rajnak, J. Chem. Phys. 49 (1968) 4412.
[31] L. Boehm, R. Reisfeld, N. Spector, J. Solid State Chem. 28 (1979) 75.
[32] Eun-Jin Cho, M. Jayasimhadri, Ki-Wan Jang, Gon Kim, Ho-Sueb Lee, J. Korean Phys. Soc. 52 (2008) 599.
[33] M. Jayasimhadri, E.J. Cho, K.W. Jang, Ho-Sueb Lee, J. Phys. D: Appl. Phys. 41 (2008) 175101.
[34] K. Patek, Glass Lasers, Butterworth, London, 1970.
[35] L.G. Clitert, L.F. Johnson, J. Chem. Phys. 44 (1966) 3514.